

Construction of mouse phantoms from segmented CT scan data for radiation dosimetry studies

This content has been downloaded from IOPscience. Please scroll down to see the full text.

2015 Phys. Med. Biol. 60 3589

(<http://iopscience.iop.org/0031-9155/60/9/3589>)

View [the table of contents for this issue](#), or go to the [journal homepage](#) for more

Download details:

IP Address: 156.111.111.162

This content was downloaded on 22/06/2015 at 19:15

Please note that [terms and conditions apply](#).

Construction of mouse phantoms from segmented CT scan data for radiation dosimetry studies

D Welch, A D Harken, G Randers-Pehrson and D J Brenner

Center for Radiological Research, Columbia University, 630 West 168th Street,
New York, NY, USA

E-mail: djb3@cumc.columbia.edu

Received 30 January 2015, revised 4 March 2015

Accepted for publication 12 March 2015

Published 10 April 2015




CrossMark

Abstract

We present the complete construction methodology for an anatomically accurate mouse phantom made using materials which mimic the characteristics of tissue, lung, and bone for radiation dosimetry studies. Phantoms were constructed using 2 mm thick slices of tissue equivalent material which was precision machined to clear regions for insertion of lung and bone equivalent material where appropriate. Images obtained using a 3D computed tomography (CT) scan clearly indicate regions of tissue, lung, and bone that match their position within the original mouse CT scan. Additionally, radiographic films are used with the phantom to demonstrate dose mapping capabilities. The construction methodology presented here can be quickly and easily adapted to create a phantom of any specific small animal given a segmented CT scan of the animal. These physical phantoms are a useful tool to examine individual organ dose and dosimetry within mouse systems that are complicated by density inhomogeneity due to bone and lung regions.

Keywords: radiation dosimetry, mouse phantom, radiographic film, micro-milling, tissue equivalent material

 Online supplementary data available from stacks.iop.org/PMB/60/093589/mmedia

(Some figures may appear in colour only in the online journal)

1. Introduction

Radiation biology experiments often utilize mice as test animals because the well-known genetic similarities within a strain provide an excellent model system for analysis. Accurate

radiation dosimetry is crucial to correctly interpret the results of such experiments. However, determining the precise dose delivered to each region within test animals is difficult to accomplish due to their intricate anatomy and the associated complex physics phenomena. Density inhomogeneity within a mouse, associated with lung and bone regions for example, complicates organ dose and dosimetry assessment (Chow *et al* 2010, Bazalova and Graves 2011). Recent work suggests that simply assigning a single dose value for a mouse irradiation is not sufficient and a comprehensive dosimetry approach which includes characterizing individual organ doses will minimize error and uncertainty (Belley *et al* 2014). Accordingly, the development of models of test animals is helpful to gain a more comprehensive understanding.

Early mathematical models of mice were developed by simply measuring the dimensions and mass of relevant features within a mouse and then modelling regions of interest using approximated spheroids, cylinders, and ellipsoids (Edmond Hui *et al* 1994). Later models have used a voxel-based approach to allow for more complex geometries. Various models have been developed from data acquired from cryosections (Bitar *et al* 2007), 3D magnetic resonance microscopy (Segars *et al* 2004, Larsson *et al* 2007, Taschereau and Chatziioannou 2007, Belley *et al* 2014), x-ray computed tomography (CT) images (Stabin *et al* 2006), or a combination of CT and cryosection data such as the widely used Digimouse model (Dogdas *et al* 2007, Boutaleb *et al* 2009, Mohammadi and Kinase 2011). These computational phantom models utilized Berger's point kernel methods or Monte Carlo methods to calculate the absorbed dose in different regions of interest. However, even with these advanced computer models and numerical methods there are still limitations to the complexity and number of interactions which can be computed.

When systems become very complex, such as in radiation biophysics, computational phantoms can become limited in their usefulness. Therefore, a next step to model the system is to replicate the experimental conditions with materials that are easier to control than the living animal. This concept of mimicking living tissue for radiation biology experiments is well established. Numerous anthropomorphic phantoms, such as the RANDO or ART models made by Alderson Radiation Therapy (Radiology Support Devices, Long Beach, CA) or the ATOM Dosimetry Phantom (Computerized Imaging Reference Systems, Norfolk, VA) are commercially available for characterizing imaging systems, quality assurance of radiation therapy, and research purposes (Gubatova *et al* 1989, Varchenya *et al* 1993, Shepherd *et al* 1997). These human phantoms are manufactured from a variety of plastics and resins to simulate soft tissue, bone, lung, and brain; they are constructed in slices and have dosimeter locations in multiple positions within the phantom organs. These anthropomorphic phantoms have been used extensively in our laboratory (Einstein *et al* 2010, 2012) and by others (Archer *et al* 1977, Sandison *et al* 1997, McDermott and Perkins 2004, Althén 2005). Recent research advances in human phantom material and construction techniques have pushed to lower the high cost of the phantoms while also improving dosimetry options (Winslow *et al* 2009).

While human phantoms are prevalent in radiological research applications, physical phantoms of animals other than humans are not widely available. The physical phantoms for other animals that are available do not offer nearly the level of detail and usefulness as their anthropomorphic counterparts. Physical mouse phantoms, for example, have had minimal development in the 50 years since Rossi *et al* filled a Lucite cylinder with tissue equivalent liquid to act as a mouse phantom (Rossi *et al* 1960). Broerse *et al* used a phantom with embedded thermoluminescent detectors, but the mouse phantoms were simply rectangular prisms (Broerse *et al* 1978). Knoess *et al* evaluated a positron emission tomograph (PET) scanner with rat and mouse phantoms which were appropriately sized cylinders, the only features of which were holes to allow insertion of a line source (Knoess *et al* 2003). Developments by Stenner *et al* used a heterogeneous mouse phantom with regions of bone simulated with hydroxyapatite

but the geometry was still limited to cylinders running the length of the phantom (Stenner *et al* 2007). Most recently, phantoms which resemble the overall shape of a mouse have been developed for fluorescence molecular tomography applications both in research applications (Joyita *et al* 2012) and commercially by PerkinElmer (XFM-2 Fluorescent Mouse Phantom, Waltham, MA); however, these fluorescent phantoms are homogeneous and lack any internal anatomical features.

In this work we demonstrate the first construction of radiation dosimetry phantoms which closely mimic the internal and overall anatomical features of a mouse. The phantoms are constructed in a method similar to the work by Winslow *et al* (Winslow *et al* 2009) where slices are processed individually and then assembled to create an entire phantom. The mouse phantoms contain regions of tissue equivalent material, bone equivalent material, and lung equivalent material and were chosen to mimic the physical properties of each region such as density and attenuation coefficients (Jones *et al* 2003, Winslow *et al* 2009). Precision computer controlled micro-milling techniques are used to replicate anatomical features down to approximately 400 μm . The described phantoms are appropriate for dosimetry studies and allow for a new method of verification in radiation biology experiments.

2. Methods

2.1. Material selection

Materials for the mouse phantom were chosen with the same goals as with previously developed human phantoms: to mimic physical properties, such as density and attenuation coefficients, and to enable simple manufacturing techniques. The mouse phantom was designed to differentiate bone regions, lung regions, and tissue regions. The model was simplified through the grouping of all regions excluding bone and lung to be classified as tissue. The innovative manufacturing process used in this work utilizes commercially available tissue equivalent material as a frame for custom mixed epoxy resin based bone equivalent material and urethane based lung tissue equivalent material.

2.2. Bone equivalent material

An epoxy resin based material developed by Jones *et al* (Jones *et al* 2003) was used to mimic bone regions within the phantom. The mixture of materials used to produce the epoxy resin is (by mass): 36.4% Huntsman Araldite GY 6010 (D. B. Becker Co., Inc., Clinton, NJ), 14.6% Jeffamine T-403 (Univar, New Rochelle, NY), 25.5% silicon dioxide (40–100 mesh sand, Thermo Fisher Scientific, Waltham, MA), and 23.5% calcium carbonate (Thermo Fisher Scientific, Waltham, MA). As in previous implementations of the bone equivalent material, the epoxy resin mixture represents a homogenous mixture of cortical and trabecular spongiosa while having a composition adjusted to match the mass density, mass attenuation coefficients, and mass energy absorption coefficients within the diagnostic energy range. Previous work with the mixture confirmed performance similar to reference values within only a few percent (Jones *et al* 2003).

2.3. Lung equivalent material

The lung tissue equivalent region of the phantom was created using the same methods employed by Winslow *et al* (Winslow *et al* 2009). Briefly, the equivalent material is made

by combining a tissue equivalent urethane-based mixture with polystyrene micro beads; the beads reduce the density of the mixture to the approximate density of the lung. The tissue equivalent mixture is produced by combining a commercially available urethane rubber compound 'PMC 121/30 Dry' (Smooth-On, Easton, PA) with 2.8% by weight of calcium carbonate (Thermo Fisher Scientific, Waltham, MA). The tissue equivalent mixture is combined with poly-fil polystyrene micro beads (Fairfield Processing, Danbury, CT) in a 10:1 ratio by weight to achieve a final lung tissue equivalent density of 0.33 g cm^{-3} .

2.4. Tissue equivalent material

All regions of the phantom which are neither bone nor lung are designated as tissue volumes. Tissue mimicking material (model number 452-202 Muscle, Gammex Inc., Middleton, WI) was obtained in a 2 mm thick sheet to be machined as required. The commercially available material is accurate for simulations using electrons and photons from 0.01 to 100 MeV.

The constructed phantoms require 1/16" diameter rods to support and align all of the slices. We utilized custom made tissue equivalent rods to maintain the correct physical response throughout the alignment rod regions. The rods were constructed by compression molding A150 tissue equivalent material into a 1/16" diameter mold.

2.5. Model preparation

We chose to create a mouse phantom designed from the Digimouse atlas data (Dogdas *et al* 2007). The Digimouse atlas is a 3D whole body mouse atlas created from CT and cryosection data of a 28 g normal nude male mouse. The openly available dataset has regions of bone, lung, tissue, and other anatomical structures precisely segmented with a voxel size of $100 \mu\text{m}$. The Digimouse atlas is commonly used for numerous modelling and simulation experiments with over 200 citations and is therefore an appropriate model to reconstruct as a phantom.

The data from the Digimouse atlas was uploaded into MATLAB (Mathworks, Natick, MA) and 2D slices were extracted in both the coronal and axial planes with a spacing of 2 mm. The spacing of slices corresponds to the thickness of the tissue mimicking material used to make each slice. A total of nine coronal slices or 40 axial slices are required to span the height or length of the mouse, respectively. An example slice in each plane is shown in figure 1. Two 1/16" circular regions were chosen and marked in each plane to allow for a tissue equivalent supporting rod to span across all of the slices to ensure proper alignment. These alignment regions were positioned to avoid lung and bone areas as much as possible. Gimp 2.8 (Gnu Image Manipulation Program, gimp.org), a free and open-source raster graphics editor, was used to merge the various slices into a single image with minimized spacing to reduce the amount of material area to be machined. Different anatomical regions could be selected across all slices as a group according to the color originally assigned by the Digimouse atlas. Thus, all of the bone, lung, alignment holes, or tissue (assumed as all regions except bone, lung, and alignment hole), could be extracted separately and saved as an image containing only those regions.

Each set of regions, now a separate image file, was individually imported as a bitmap into Inkscape, (The Inkscape Team, inkscape.org), a free and open-source vector graphics editor. Using Inkscape, the bitmap file was first traced to create a vector image which indicated the regions which needed to be removed to create each anatomical region. The vector image was processed to create an appropriate gcode output for computer aided machining using the Gcodetools version 1.7 plugin. The generated gcode accounts for the width of the end-mill to be used during machining, therefore, features of the vector image smaller than the tool width are excluded from the machining process.

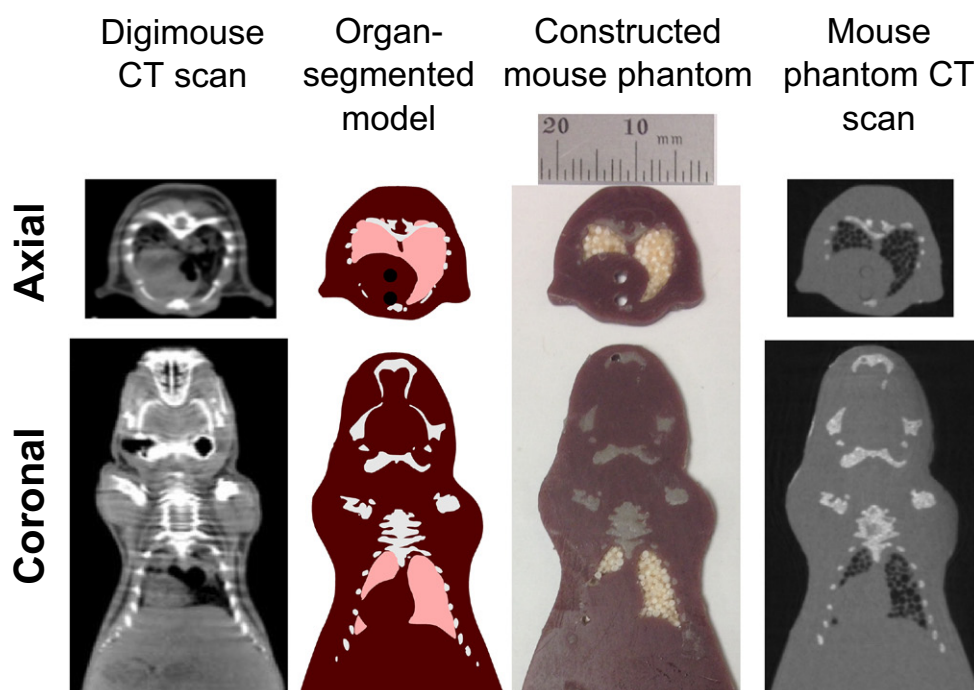


Figure 1. The progression from CT scan of a mouse, to an organ-segmented digital model, to constructed phantom, to verification by CT scan is exhibited for representative slices in both the axial and coronal planes. The CT topograms in the left column were obtained to create the Digimouse model (Dogdas *et al* 2007). The Digimouse model allowed segmentation of relevant organ and tissue data, exhibited in the second column; regions of tissue, lung, bone, and alignment rod are included. The third column displays photographs of slices of the constructed phantom. Topograms obtained from CT scans of the mouse phantom are shown in the right column. All of the coronal images have been cropped to maintain the same scale as the axial images. The minor differences between the original Digimouse CT scan and the organ segmented model are due to the use of a common coordinate system with the cryosection and PET data during organ segmentation; sole use of the CT scan data for segmentation would eliminate these inconsistencies.

2.6. Machining and assembly

Precision machining was performed using a Minitex Mini-Mill/3 micro-milling machine (Minitex Machinery, Norcross, GA) running Mach3 control software. The end mill used during all machining steps was a carbide plastic-cutting end mill with two flutes; the size used, 0.397 mm diameter with a 3.175 mm length of cut (60 125, Harvey Tool, Rowley, MA), was the minimum diameter end mill with a length which would allow for a complete cut through the 2 mm of tissue equivalent plastic. The end mill was run at 25 000 RPM with a feed rate of 300 mm min⁻¹.

Machining of the phantom began with a 10 cm by 20 cm area of tissue equivalent material, which is sufficient for fabrication of one mouse. The first areas milled from the tissue sheet were the lung regions. After lung region removal, a small amount of candle wax was dripped into each region to act as placeholder during the remaining manufacturing steps. Next, the alignment hole regions were milled and subsequently filled with a different color candle wax. Finally, the bone regions were milled away followed by milling steps to free

each slice from the sheet of tissue material by milling out the total tissue regions. Filling the bone regions with wax was not necessary because they would be the first to be filled with equivalent material.

Bone equivalent material was mixed as described and allowed to sit for 6–8 h prior to application to allow it to partially cure and therefore thicken. The bone material was squeegeed across each piece until all bone regions were filled; the higher viscosity of the slightly cured epoxy permitted easier filling of larger bone regions. After verifying that each bone region was filled, a piece of tape was placed across the bottom side of the slice to prevent epoxy from running out. Excess bone equivalent material was cleaned off and the pieces were allowed an additional 36 h to fully cure. Next, the placeholder wax for the lung regions was removed and each region was over-filled with the lung equivalent material and cured overnight. Upon curing, excess lung material was cut away to leave the lung surfaces even with the remainder of the slice. Finally, the placeholder wax in the alignment holes was removed and all of the pieces could be assembled and held together using 1/16" diameter tissue equivalent rods as shown in figure 2.

2.7. CT image acquisition

A Quantum FX micro CT Imaging System (PerkinElmer, Waltham, MA) was used to obtain CT image data from the completed mouse phantoms. Each phantom was scanned using a 270 s scan which generated 3D tomography data with a voxel size of 148 μm .

2.8. Film dosimetry measurement

The completed mouse phantom was tested for use in dosimetry measurements using Gafchromic radiographic films (Ashland, Covington, KY). Gafchromic EBT3 film was used for testing. The film has a total thickness of 280 μm made up of a 30 μm active region with a 125 μm polyester base coating on either side. Holes were drilled through the film to allow placement between slices in a secured position using the alignment rods. For demonstration purposes, the EBT3 film was placed between the third and fourth coronal slice counting from the ventral side (6 mm from the bottom of the phantom); the remaining six coronal slices were located above the film. A Westinghouse x-ray machine, operating at 100 kVp and 10 mA without added filtration, was used to irradiate. The phantom and film were irradiated to a nominal 70 cGy pulmonary dose of x-rays at a distance of 50 cm and a rate of 38.7 cGy min^{-1} as determined using a Victoreen R-meter. The x-ray source and phantom were oriented to irradiate from the dorsal side, thus the film was perpendicular to the x-ray source. After exposure, films were scanned using an Epson Perfection V700 Photo flatbed scanner (Epson, Suwa, NGN, Japan) and processed using FilmQA Pro software (Ashland, Covington, KY). All three color channels were used for calibration and subsequent dose mapping to obtain optimum results which are corrected for nonuniformities in the active film as well as scanner related artifacts (Micke *et al* 2011).

3. Results

3.1. Completed mouse phantom

Two completed mouse phantoms are shown in figure 2. The weight of each completed phantom is 24 g. Example slices from each of the phantoms are shown in figure 1. The photograph of the slices from the phantom exhibits regions of bone and lung in the appropriate positions

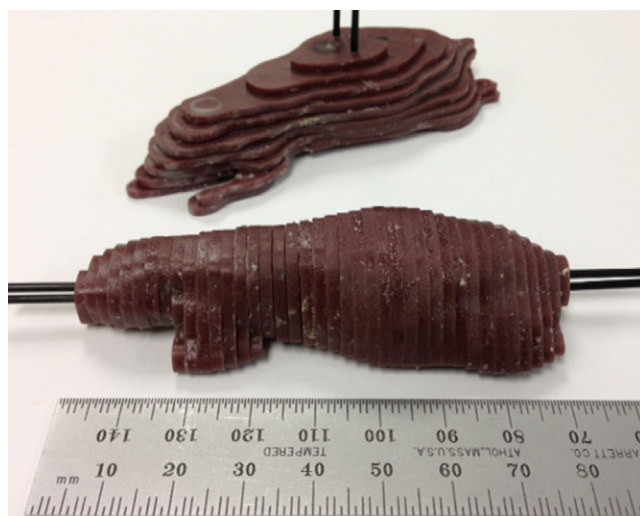


Figure 2. The two constructed mouse phantoms, one made with coronal slices (top) and one with axial slices (bottom), are shown completely assembled. The coronal sliced phantom is made of nine slices and the axial sliced phantom contains 40 slices. Slices are held in place by two tissue equivalent supporting rods running perpendicular to the slice plane.

within the tissue equivalent plastic. The precision milling allowed for intricate details to be replicated while also ensuring their exact positioning within the phantom.

Machining and assembly of a complete mouse phantom could be completed over a period of approximately four days. Construction time consisted of approximately 12 h of combined machining time for all steps; the remainder of the four days was required for application and subsequent curing of the lung and bone regions. All slices were constructed in parallel which ensured consistent material properties throughout the phantoms. We confirmed the densities of both the lung equivalent and bone equivalent material are in agreement with the values measured in the original work using these exact formulations by Winslow *et al* (Winslow *et al* 2009) and Jones *et al* (Jones *et al* 2003), respectively.

3.2. CT imaging

Example topograms from a 3D CT scan of each of the mouse phantoms are shown in the right column of figure 1. The topograms display distinct regions of lung and bone equivalent material within tissue equivalent material. Complete 3D topograms which scan each mouse phantom perpendicular to their respective slice orientation are available in the supplementary material (stacks.iop.org/PMB/60/093589/mmedia).

3.3. Film dosimetry

The result of radiographic film dosimetry with the constructed mouse phantoms is shown in figure 3. The use of the FilmQA Pro software enabled multichannel dosimetry calibration and application of the calibration information to a given film. The grayscale dose map shows the various doses of 100 kVp x-rays received across an entire coronal slice of a phantom. The high resolution of the film allows for various dose profiles to be acquired; profiles which

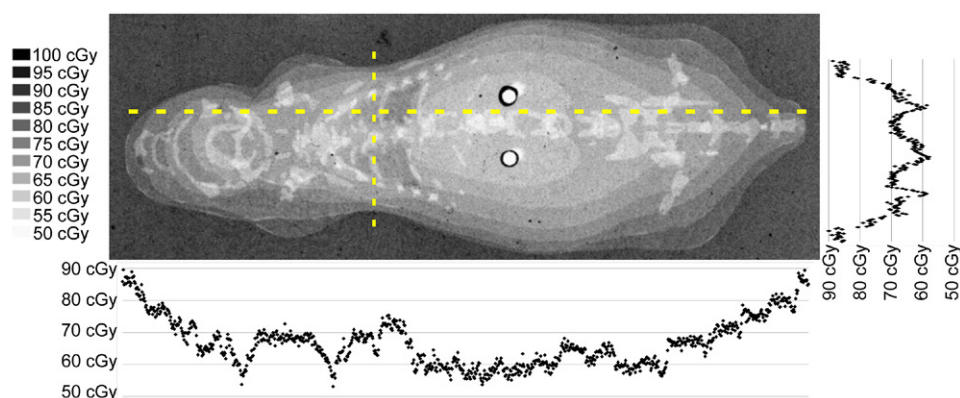


Figure 3. The grayscale dose map obtained from the radiographic film shows variations in absorbed dose across the coronal phantom when exposed to a nominal 70cGy pulmonary dose of 100kVp x-rays. Plots of the dose profile along the dashed lines are aligned with their position in the dose map.

pass through the lung region of the mouse phantom are shown in the figure to illustrate this capability.

4. Discussion

The constructed mouse phantoms are unique to radiation dosimetry studies because they exhibit precision placement of equivalent material throughout the model. CT scans and radiographic films clearly exhibit these extensive details incorporated into the phantom. The phantoms are robust, easily handled, and are easily disassembled. Additionally, the modular nature of the phantoms allows for the insertion of ‘dummy’ slices if desired; these slices would be identical in shape and material to the original slices but would include access ports for insertion of dosimeters such as microMOSFETs (Best Medical Ltd., CA) or TLD chips (Thermo Fisher Scientific, Waltham, WA). The phantom described here contains regions of bone and lung, which are considered the most important in radiation dosimetry due to the large difference in density compared to tissue. Due to the modular nature of the phantom, it would be easy to fabricate additional slices containing a different organ of interest for more specialized studies.

The thickness of commercially available tissue equivalent plastic sheets limits the level of detail within a phantom our construction method can achieve. A thinner sheet would allow for a greater number of slices and therefore more resolution orthogonal to slice direction. A thinner sheet also reduces the required length of the end mill to completely cut through; smaller diameter end mills become available at the shorter lengths therefore smaller features can be created. Reduction of slice thickness is therefore necessary if finer details are required than those within the presented phantoms. Finer detail throughout the model would permit examination of variations in dose due to inhomogeneity across smaller regions; for example, varying the internal bone structure to represent cortical and trabecular spongiosa regions in an anatomically correct configuration instead of a single homogenous structure. Current research of dose variation within bone regions is limited to Monte Carlo simulations and would be aided with the addition of validation using a physical model. Likewise, future studies which include Monte Carlo computer simulations of the mouse phantoms presented in this work will provide additional verification of their functionality.

The construction method presented here utilizes commercially available tissue equivalent material. Manufacturing a phantom requires fewer steps than the methods of Winslow *et al* (Winslow *et al* 2009). The quick construction time and relatively low cost of materials grants the opportunity to create individualized phantoms for a given experiment. Furthermore, the methods presented here are applicable to other small animals such as rats. These advantages can allow widespread and customized use of small animal phantoms across radiation biology experiments.

5. Conclusions

To the best of our knowledge, this is the first construction of a heterogeneous mouse phantom with tissue, bone, and lung equivalent material. This is also the first mouse phantom developed which replicates the correct configuration of these multiple anatomical regions. By using materials with properties similar in behavior to those of native materials, we have created phantoms suitable for radiological experimentation. These physical models are therefore useful in verification of many of the mathematical models for radiation biology experiments using the same initial CT scan dataset. Furthermore, the mouse phantoms can be used in place of live mice to easily and quickly measure absorbed dose using radiographic film for dosimetry. The construction methodology presented here can be readily adapted to create a phantom of any specific small animal given a segmented CT scan of the animal. This potential for an individualized phantom can allow customized analysis of radiation experiments and specific verification of results.

Acknowledgments

The authors would like to thank Christopher Damoci for his assistance in CT data acquisition at the Herbert Irving Comprehensive Cancer Center Small Animal Imaging Shared Resource facility. We also wish to thank Gary Johnson for manufacturing the tissue equivalent support rods. This work was supported by grant number U19-AI067773 to the Center for High-Throughput Minimally Invasive Radiation Biodosimetry from the National Institute of Allergy and Infectious Diseases (NIAID) National Institutes of Health (NIH). The content is solely the responsibility of the authors and does not necessarily represent the official views of the NIAID or NIH.

References

- Althén J N 2005 Automatic tube-current modulation in CT—a comparison between different solutions *Radiat. Prot. Dosim.* **114** 308–12
- Archer B R, Glaze S, North L B and Bushong S C 1977 Dosimeter placement in the Rando phantom *Med. Phys.* **4** 315–8
- Bazalova M and Graves E E 2011 The importance of tissue segmentation for dose calculations for kilovoltage radiation therapy *Med. Phys.* **38** 3039–49
- Belley M D, Wang C, Nguyen G, Gunasingha R, Chao N J, Chen B J, Dewhirst M W and Yoshizumi T T 2014 Toward an organ based dose prescription method for the improved accuracy of murine dose in orthovoltage x-ray irradiators *Med. Phys.* **41** 034101–7
- Bitar A, Lisbona A, Thedrez P, Maurel C S, Forestier D L, Barbet J and Bardies M 2007 A voxel-based mouse for internal dose calculations using Monte Carlo simulations (MCNP) *Phys. Med. Biol.* **52** 1013–25

- Boutaleb S, Pouget J P, Hindorf C, Pelegrin A, Barbet J, Kotzki P O and Bardies M 2009 Impact of mouse model on preclinical dosimetry in targeted radionuclide therapy *Proc. IEEE* **97** 2076–85
- Broerse J, Zoetelief J and Puite K 1978 Dosimetry intercomparisons for evaluation of late effects of ionizing radiation *Acta Oncol.* **17** 225–34
- Chow J C L, Leung M K K, Lindsay P E and Jaffray D A 2010 Dosimetric variation due to the photon beam energy in the small-animal irradiation: a Monte Carlo study *Med. Phys.* **37** 5322–9
- Dogdas B, Stout D, Chatziioannou A F and Leahy R M 2007 Digimouse: a 3D whole body mouse atlas from CT and cryosection data *Phys. Med. Biol.* **52** 577–87
- Edmond Hui T, Fisher D R, Kuhn J A, Williams L E, Nourigat C, Badger C C, Beatty B G and David Beatty J 1994 A mouse model for calculating cross-organ beta doses from yttrium-90-labeled immunoconjugates *Cancer* **73** 951–7
- Einstein A J, Elliston C D, Arai A E, Chen M Y, Mather R, Pearson G D, DeLaPaz R L, Nickoloff E, Dutta A and Brenner D J 2010 Radiation dose from single-heartbeat coronary CT angiography performed with a 320-detector row volume scanner 1 *Radiology* **254** 698–706
- Einstein A et al 2012 Effect of bismuth breast shielding on radiation dose and image quality in coronary CT angiography *J. Nucl. Cardiol.* **19** 100–8
- Gubatova D, Varchenya V and Krastinya A 1989 Tissue-equivalent phantoms in radiological protection *Kernenergie* **32** 10–3
- Jones A K, Hintenlang D E and Bolch W E 2003 Tissue-equivalent materials for construction of tomographic dosimetry phantoms in pediatric radiology *Med. Phys.* **30** 2072–81
- Joyita D, Sangtae A, Changqing L, Simon R C and Richard M L 2012 Joint L^1 and total variation regularization for fluorescence molecular tomography *Phys. Med. Biol.* **57** 1459–76
- Knoess C, Siegel S, Smith A, Newport D, Richerzhagen N, Winkeler A, Jacobs A, Goble R, Graf R, Wienhard K and Heiss W-D 2003 Performance evaluation of the microPET R4 PET scanner for rodents *Eur. J. Nucl. Med. Mol. Imag.* **30** 737–47
- Larsson E, Strand S-E, Ljungberg M and Jönsson B-A 2007 Mouse S-factors based on Monte Carlo simulations in the anatomical realistic Moby phantom for internal dosimetry *Cancer Biother. Radiopharm.* **22** 438–42
- McDermott L and Perkins A 2004 Comparison of measured and calculated radiotherapy doses in the chest region of an inhomogeneous humanoid phantom *Australas. Phys. Eng. Sci. Med.* **27** 16–21
- Micke A, Lewis D F and Yu X 2011 Multichannel film dosimetry with nonuniformity correction *Med. Phys.* **38** 2523–34
- Mohammadi A and Kinase S 2011 Influence of voxel size on specific absorbed fractions and s-values in a mouse voxel phantom *Radiat. Prot. Dosim.* **143** 258–63
- Rossi H H, Bateman J L, Bond V P, Goodman L J and Stickley E E 1960 The dependence of RBE on the energy of fast neutrons: 1. Physical design and measurement of absorbed dose *Radiat. Res.* **13** 503–20
- Sandison G A, Papiez E, Bloch C and Morphis J 1997 Phantom assessment of lung dose from proton arc therapy *Int. J. Radiat. Oncol. Biol. Phys.* **38** 891–7
- Segars W P, Tsui B M W, Frey E C, Johnson G A and Berr S S 2004 Development of a 4-D digital mouse phantom for molecular imaging research *Mol. Imag. Biol.* **6** 149–59
- Shepherd S F, Childs P J, Graham J D, Warrington A P and Brada M 1997 Whole body doses from linear accelerator-based stereotactic radiotherapy *Int. J. Radiat. Oncol. Biol. Phys.* **38** 657–65
- Stabin M G, Peterson T E, Holburn G E and Emmons M A 2006 Voxel-based mouse and rat models for internal dose calculations *J. Nucl. Med.* **47** 655–9
- Stenner P, Berkus T and Kachelriess M 2007 Empirical dual energy calibration (EDEEC) for cone-beam computed tomography *Med. Phys.* **34** 3630–41
- Taschereau R and Chatziioannou A F 2007 Monte Carlo simulations of absorbed dose in a mouse phantom from 18-fluorine compounds *Med. Phys.* **34** 1026–36
- Varchenya V, Gubatova D, Sidorin V and Kalnitsky S 1993 Children's heterogeneous phantoms and their application in röntgenology *Radiat. Prot. Dosim.* **49** 77–8
- Winslow J F, Hyer D E, Fisher R F, Tien C J and Hintenlang D E 2009 Construction of anthropomorphic phantoms for use in dosimetry studies *J. Appl. Clin. Med. Phys.* **10** 2986